Molecular simulation of Rayleigh-Brillouin scattering in binary gas mixtures and extraction of the rotational relaxation numbers

Qihan Ma,[1] Chunxin Yang,[1] Domenico Bruno,[2] and Jun Zhang[1,*]

[1]*School of Aeronautic Science and Engineering, Beihang University, Beijing 100191, China*

[2]*Istituto per la Scienza e Tecnologia dei Plasmi (ISTP)-CNR, via G. Amendola, 122/D, 70126 Bari, Italy*

(Received 24 June 2021; accepted 31 August 2021; published 27 September 2021)

Rayleigh-Brillouin scattering (RBS) in gases has received considerable attention due to its applications in LIDAR (light detection and ranging) remote sensing and gas property measurements. In most cases, the RBS spectra in the kinetic regime are calculated based on kinetic model equations, which are difficult to be applied to complex gas mixtures. In this work, we employ two widely used molecular simulation methods, i.e., direct simulation Monte Carlo (DSMC) and molecular dynamics (MD), to calculate the spontaneous RBS spectra of binary gas mixtures. We validate these two methods by comparing the simulation results for mixtures of argon and helium with the experimental results. Then we extend the RBS calculations to gas mixtures involving polyatomic gases. The rotational relaxation numbers specific to each species pair in DSMC are determined by fitting the DSMC spectra to the MD spectra. Our results show that all the rotational relaxation numbers for air composed of N_2 and O_2 increase with temperature in the range of 300–750 K. We further calculate the RBS spectra for binary mixtures composed of N_2 and one noble monatomic gas, and the simulation results show that the rotational relaxation of N_2 is greatly affected by the mass of the noble gas atoms. This work demonstrates that RBS is a promising and alternative way to study the rotational relaxation process in gas mixtures.

DOI: 10.1103/PhysRevE.104.035109

I. INTRODUCTION

With the rapid development of laser techniques and high-resolution spectroscopy, Rayleigh-Brillouin scattering (RBS) in gases has received considerable attention due to its applications in LIDAR (light detection and ranging) remote sensing [1–3] and gas property measurements [4–9]. One of the recent well-known applications of RBS is the measurement of global wind profiles by the ADM-Aeolus mission of the European Space Agency (ESA) [2,3]. Generally, there are two typical types of RBS, i.e., spontaneous RBS and coherent RBS. The former arises from the gas density fluctuations due to random thermal motion of molecules [9,10], while the latter arises from the gas density fluctuations induced by an optical dipole force [11,12]. The spectral profile of RBS contains abundant information on gas properties, such as temperature, sound speed, thermal conductivity, and bulk viscosity [13,14]. These properties can be retrieved by comparing the calculated RBS spectra with the experimental ones [8,15,16].

According to the RBS theory, light scattering with the characteristic wavelength L and frequency f represents the measured fluctuations with the same wavelength and frequency [13]. The shapes of the RBS spectra under different conditions can be characterized by a dimensionless parameter Y, which is defined as the ratio of L to the molecular mean free path λ [4,9],

$$Y = \frac{L}{2\pi\lambda} = \frac{1}{q\lambda}, \tag{1}$$

where q is the scattering wave number; i.e., $q=\frac{2\pi}{L}$. For $Y \gg 1$ or $Y \ll 1$, the gas is in the hydrodynamic or the free molecular regime, and the RBS spectra can be calculated based on the fluctuating Navier-Stokes-Fourier equations [13,14] and the collisionless Boltzmann-type equation [11], respectively. On the contrary, it is challenging to determine the RBS spectra for $Y \approx 1$; that is, the molecular mean free path is comparable to the fluctuation wavelength, and this situation is referred to as the kinetic regime. Theoretically, the dynamics of gas molecules in this regime can be described by the full Boltzmann equation for monatomic gases and the Wang-Chang-Uhlenbeck (WCU) equation for polyatomic gases [6]. Owing to the great complexity of the Boltzmann-type collision integral, in most cases the RBS spectra are calculated based on kinetic model equations.

For monatomic gases, previous research has shown that the RBS line shape can be obtained by solving kinetic model equations based on the linearized Boltzmann equation [17,18]. For polyatomic gases, a variety of kinetic models have been proposed so far based on the WCU equation [19–21]. Among these models, the Tenti S6 model [19] is the most prevailing and has been used to calculate the RBS spectra of various gases [7,22,23]. This model needs three parameters relevant to the transport properties of the gas to determine the RBS spectral shape: thermal conductivity κ, shear viscosity μ_s, and bulk viscosity μ_b. Particularly, μ_b is directly related to the relaxation times τ_{int} [8,24,25] of the molecular internal energy modes, which is hard to measure experimentally, and it is a promising way to determine μ_b by fitting the calculated RBS spectra to the experimental ones [22]. It should be noted that in the current RBS experiments, the

*jun.zhang@buaa.edu.cn

 ©2021 American Physical Society

frequency of sound at the light scattering wavelength is generally on the order of gigahertz, indicating that the timescale of measured fluctuations ($\sim 10^{-9}$ s) is much shorter than the vibrational relaxation time τ_{vib} ($\sim 10^{-6}$ s) [7,8]. Therefore, it is reasonably assumed that RBS spectra are only dependent on the relaxation of rotational energy, as the vibrational modes remain "frozen" in the measured timescale.

Note that the aforementioned kinetic models are limited to one-component gases. For monatomic gas mixtures, a previous study has reported that the RBS spectra can be obtained from kinetic models based on linearized Boltzmann equations [26]. Later, Bonatto and Marques [27] proposed a new model by simplifying the Boltzmann collision operators to simple relaxation-time terms, and they obtained the RBS spectra in good agreement with the experimental results reported by Gu *et al.* [28]. For mixtures containing molecular gases, however, there is still a lack of effective kinetic models for calculating RBS spectra. Recently, Wang *et al.* [29] proposed a generalized hydrodynamic model based on the moment method, and applied it to the calculation of the RBS spectra for binary mixtures of SF_6-He, SF_6-D_2, and SF_6-H_2. Note that this model is only applicable to the case of a mixture with heavy and light disparate masses [29]. In addition, this model uses a single relaxation number, which is defined as the ratio of the mean rotational relaxation time to the mean collision time, as the fitting parameter. Therefore, it cannot distinguish the rotational relaxation process specific to different species for gas mixtures [30,31].

In order to overcome the limitations of the available model equations, two widely used molecular simulation methods, namely, the direct simulation Monte Carlo (DSMC) [31,32] and the molecular dynamics (MD) [33] methods, are employed in this paper to calculate RBS spectra. By using molecular simulation approaches, not only will the interactions between molecules be more accurately described, but the RBS calculations can be extended to more complex gas mixtures involving polyatomic gases.

DSMC is a stochastic method which simulates the motions and collisions of a large number of representative molecules. It has been demonstrated that for monatomic gases the DSMC solutions can converge to those of the Boltzmann equation [34]. Over the past 50 years, the DSMC method has been proved to be a powerful tool for the simulation of one-component gas and gas mixtures, covering the whole fluid regimes from the free molecular to the hydrodynamic limit [32,35–37]. Recently, the method has been used to calculate the RBS spectra of one-component monatomic/molecular gases [38,39] and noble gas mixtures [40]. For molecular gases, the Borgnakke-Larsen (BL) model [41] is popularly employed in DSMC to describe the rotational-translational (RT) energy exchange. The so-called rotational relaxation number, which is directly related to the rotational relaxation time [31], can be obtained by fitting the DSMC calculated RBS line shapes to the experimental ones [39].

Unlike DSMC, the MD method is a deterministic simulation method, as the movement of the simulation molecules strictly follows Newton's equations of motion [33]. Moreover, the MD method uses interatomic potentials instead of phenomenological collision models to accurately describe the interactions between atoms and molecules [33].

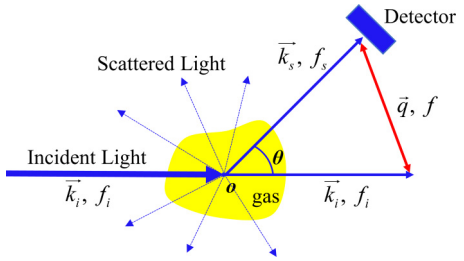

FIG. 1. Schematic of the spontaneous RBS experiments. $\vec{q}$ and f represent the scattering wave vector and frequency in both directions for Stokes and anti-Stokes scattering.

Therefore, the MD simulation results could be considered as the standard if the interatomic potentials or the potential energy surfaces (PESs) of the system are accurately predetermined. By comparing DSMC results with MD results, one can determine the parameters used in the DSMC phenomenological models, and even make further improvements to the models [36,42,43]. Up to now, the MD method has only been used to study the RBS of pure Ar and CO_2 in the kinetic regime [44].

In this work we employ DSMC and MD methods to calculate the spontaneous RBS spectra of binary gas mixtures. Our aim is to break through the limitations of the existing kinetic models for RBS calculation, and at the same time to provide an alternative way to study the rotational relaxation process in multicomponent gases. As a benchmark test, the MD and DSMC results are first compared to the experimental results [28] for mixtures of Ar and He without any fitting parameters. Then we extend our calculations to mixtures involving molecular gases, which have not been studied very much before. Using an appropriate pair selection algorithm in DSMC [30], we extract the rotational relaxation numbers specific to each species pair by fitting the RBS spectra obtained by DSMC with the ones determined by MD. Specifically, we calculate the RBS spectra of air composed of N_2 and O_2 for temperatures up to 750 K, and the variation of the rotational relaxation numbers against the temperature is determined. Meanwhile, we calculate the RBS spectra of binary mixtures composed of N_2 and one noble monatomic gas, and the effect of noble gas atoms on the rotational relaxation of N_2 is further discussed.

The remainder of this paper is organized as follows: In Sec. II, we introduce the basic theory of spontaneous RBS. In Sec. III, we first introduce the general calculation procedure for RBS spectra, then we present the simulation details of DSMC and MD methods. In Sec. IV, the calculation results of Ar-He gas mixtures are first presented; then we extend our research to more complex gas mixtures, i.e., the air and the nitrogen-noble gas mixtures. Conclusions are drawn in Sec. V.

II. SPONTANEOUS RAYLEIGH-BRILLOUIN SCATTERING

Figure 1 shows the schematic diagram of the spontaneous RBS experiments. The incident light with wave vector $\vec{k}_i$ and frequency f_i is scattered by the gas medium, and the scattered light with wave vector $\vec{k}_s$ and frequency f_s is received by the detector. For RBS calculations, we mainly focus on the

characteristic wave vector $\vec{q}$ and frequency f of the scattering process, whose magnitude can be calculated as [14,45]

$$|\vec{q}| = q = |\vec{k}_i - \vec{k}_s|, \tag{2}$$

$$|f| = |f_i - f_s|, \tag{3}$$

where q is the scattering wave number. Since in RBS experiments we have $|\vec{k}_i| \approx |\vec{k}_s|$ [14,45], q can be expressed as [14]

$$q = 2|\vec{k}_i| \sin\left(\frac{\theta}{2}\right) = \frac{4\pi\hat{n}}{\lambda_{\text{in}}} \sin\left(\frac{\theta}{2}\right), \tag{4}$$

where $\lambda_{\text{in}} = \frac{2\pi\hat{n}}{|k_i|}$ is the incident wavelength, $\hat{n}$ is the refractive index, and θ is the scattering angle.

Spontaneous RBS arises from the isotropic part of the local dielectric constant fluctuation $\delta\varepsilon(\vec{r}, t)$ [9]. Assuming that the gas medium is in equilibrium without any macroscopic velocity, the RBS spectral distribution can be expressed as [14]

$$S(\vec{q}, f) = \int_{-\infty}^{+\infty} \langle \delta\varepsilon^*(\vec{q}, 0)\delta\varepsilon(\vec{q}, t)\rangle e^{-i(2\pi f)t} dt, \tag{5}$$

where $\delta\varepsilon(\vec{q}, t)$ is the spatial Fourier transform of $\delta\varepsilon(\vec{r}, t)$ with respect to $\vec{q}$; $\langle \delta\varepsilon^*(\vec{q}, 0)\delta\varepsilon(\vec{q}, t)\rangle$ denotes the time autocorrelation function of $\delta\varepsilon(\vec{q}, t)$. For a gas mixture containing s components, the $\delta\varepsilon(\vec{r}, t)$ is related to the spontaneous fluctuations of partial number densities $\delta n_i(\vec{r}, t)$ via the Clausius-Mossotti relation [27,40,46]:

$$\delta\varepsilon(\vec{r}, t) = \sum_{i=1}^{s} \hat{\alpha}_i \delta n_i(\vec{r}, t), \tag{6}$$

where $\hat{\alpha}_i$ denotes the atomic or molecular polarizability of the ith species. Substituting Eq. (6) into Eq. (5) yields

$$S(\vec{q}, f) = \sum_{i=1}^{s}\sum_{j=1}^{s} \hat{\alpha}_i\hat{\alpha}_j \delta n_i^*(\vec{q}, f)\delta n_j(\vec{q}, f), \tag{7}$$

where $\delta n_i(\vec{q}, f)$ denotes the space-time Fourier transform of $\delta n_i(\vec{r}, t)$ with respect to $(\vec{q}, f)$. For one-component gases, Eq. (7) can be simplified to

$$S(\vec{q}, f) = \hat{\alpha}^2 |\delta n(\vec{q}, f)|^2. \tag{8}$$

As mentioned in Sec. I, the RBS line shapes can be characterized by a dimensionless parameter Y [see Eq. (1)]. It can be seen from Fig. 2, for a large Y value, that the central Rayleigh peak and two Brillouin peaks are clearly separated. The Rayleigh peak arises from the scattering of light from entropy fluctuations, while the Brillouin peaks represent the light scattering from sound waves [9,13]. As Y becomes smaller, the collective effect of the gas becomes weaker, and the Brillouin peaks associated with the sound waves are difficult to detect from the RBS. For $Y \ll 1$, the gas is in the limit of free molecular flow; the shape of the RBS spectrum is a Gaussian curve corresponding to the Maxwellian velocity distribution of the molecules [4,9,47].

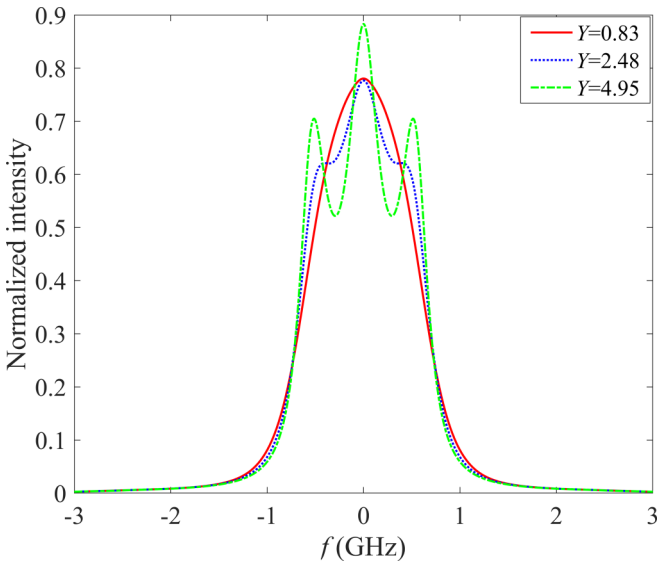

FIG. 2. RBS spectra of argon gas corresponding to different Y values. The spectra are obtained using the DSMC method (see Sec. III A). Y is increased by changing pressure P from 0.5 to 3 bars, while the other parameters are fixed ($\lambda_{\text{in}} = 403$ nm, $\theta = 40°$, $T = 300$ K).

III. SIMULATION METHODS

In this paper, we employ both DSMC and MD methods for RBS calculations. The general calculation procedure is shown in Fig. 3. The gas in equilibrium without any macroscopic velocity is simulated. To prevent acoustic standing waves [10,44], periodic boundary conditions are assumed in all three directions.

Due to the isotropic nature of density fluctuations, it is efficient to sample them only in one dimension [33,39]. Specifically, for all the simulations in this work, the length in the y direction is chosen as the scattering wavelength L, while the lengths of the other two directions are arbitrary, to control the total number of simulated particles. To obtain the density fluctuations of each species i at different space and time points, i.e., $\delta n_i(y, t)$, the computational domain is divided into 64 bins in the y direction, and the instantaneous density fluctuations are obtained at 1024 discrete time points for each space bin. Then the fast Fourier transform (FFT) is applied to the space-time data of $\delta n_i(y, t)$ to determine the RBS spectra $S(\vec{q}, f)$, as presented in Eq. (7).

For the sake of comparison, the time sampling of $\delta n_i(y, t)$ should be elaborately controlled to make the frequencies of the calculated spectra close to those reported in experiments [22,28]. Specifically, the sampling time interval is smaller than 0.132 ns to ensure that the half-frequency range of the spectrum is larger than 3.78 Ghz, and the total sampling time is longer than 20 ns to ensure that the frequency resolution of the spectrum is less than 0.05 Ghz.

In order to reduce the signal-to-noise ratio of the RBS spectra, a large number of independent runs is performed and the ensemble average is used. The number of independent runs is about 9000 for DSMC simulations and 5000 for MD simulations, for a compromise between the calculation accuracy and simulation cost.

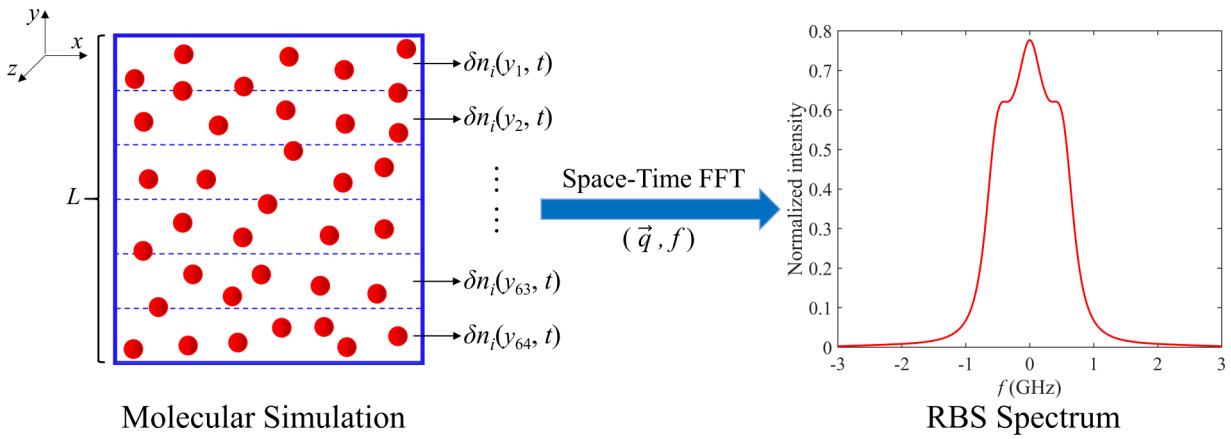

FIG. 3. Schematic of the RBS calculation procedure. The simulation domain is displayed in the *x*-*y* plane.

The basic molecular properties for both DSMC and MD simulations are listed in Table I. Other simulation details for DSMC and MD methods are introduced in the following.

A. Direct simulation Monte Carlo method

In DSMC, each calculation time step implements two sequential processes, i.e., molecular movements and intermolecular collisions. While the molecular movements are performed deterministically according to molecular instantaneous velocities, the intermolecular collisions are treated stochastically using phenomenological models including elastic and inelastic collisions [31,32].

In this work, the variable soft sphere (VSS) molecular model [49] is used for the modeling of elastic collisions. Three parameters, d_{ref}, ω, and α, need to be specified for a collision pair using the VSS model. Specifically, d_{ref} is the reference collision diameter at a reference temperature (T_{ref}), which can be directly related to the total collision cross section. ω represents the dependence of the collision diameter d on the kinetic energy of the collision pair, and α represents the scattering angle distribution of the collision. With predetermined values of these three parameters, the VSS model is capable of reproducing the experimental values of diffusion coefficient D and shear viscosity μ_s [31,32]. The data of VSS parameters for like-species pairs (i-i) are extracted from Ref. [32], and they are presented in Table II.

For gas mixtures, the VSS parameters for unlike-species pairs (i-j) are shown in Table III. The $d_{\text{ref},i\text{-}j}$ is assumed to be equal to the mean value of $d_{\text{ref},i\text{-}i}$ and $d_{\text{ref},j\text{-}j}$ [32]. The $\omega_{i\text{-}j}$ is also assumed as the mean value of $\omega_{i\text{-}i}$ and $\omega_{j\text{-}j}$ [32], except for the $\omega_{\text{He-Ar}}$, which is directly extracted from Ref. [32]. For the determination of $\alpha_{i\text{-}j}$, $\alpha_{\text{He-Ar}}$, $\alpha_{\text{N}_2\text{-O}_2}$, and $\alpha_{\text{N}_2\text{-Ar}}$ are directly extracted from Ref. [32], while the others are calculated as [32]

$$\alpha_{i-j} = \frac{8(5-2\omega_{i\text{-}j})nD_{\text{ref},i\text{-}j}\pi(d_{\text{ref},i\text{-}j})^2}{3(2\pi k_B T_{\text{ref}}/m_r)^{0.5}} - 1, \tag{9}$$

where $D_{\text{ref},i\text{-}j}$ is the reference diffusion coefficient at $T_{\text{ref}} = 273.15$ K, k_B is the Boltzmann constant, and m_r is the reduced mass. n is the total number density of the mixture, which is calculated by $P/k_B T_{\text{ref}}$ under standard conditions.

Once the VSS model parameters are determined, we can calculate the mean collision rate of species i for gas mixtures in equilibrium [32],

$$\nu_i = \sum_{j=1}^{s} \nu_{i\text{-}j} = \sum_{j=1}^{s} [2\sqrt{\pi}(d_{\text{ref},i\text{-}j})^2 n_j (T/T_{\text{ref}})^{1-\omega_{i\text{-}j}} \times (2k_B T_{\text{ref}}/m_r)^{0.5}], \tag{10}$$

where $\nu_{i\text{-}j}$ is the mean collision rate between species i and species j, and n_j denotes the partial number density of species j. Then the mean collision rate for the mixture can be defined as [32]

$$\nu = \sum_{i=1}^{s} \frac{n_i}{n} \nu_i, \tag{11}$$

TABLE I. Basic molecular properties for the simulations.

Molecule	Mass (amu)	Average polarizability (10^{-40} C m^2 V^{-1})[a]
He	4.0	0.227
Ne	20.2	0.439
Ar	39.9	1.82
Kr	83.8	2.94
Xe	131.3	4.50
N_2	28.0	1.94
O_2	32.0	1.75

[a]The polarizabilities of He, Ar, and Kr are obtained from Ref. [28]. Others are obtained from Ref. [48].

TABLE II. VSS parameters for like-species pairs [32] ($T_{\text{ref}} = 273.15$ K).

Species type (i)	$d_{\text{ref},i\text{-}i}$ (Å)	$\omega_{i\text{-}i}$	$\alpha_{i\text{-}i}$
He	2.30	0.66	1.26
Ne	2.72	0.66	1.31
Ar	4.11	0.81	1.40
Kr	4.70	0.8	1.32
Xe	5.65	0.85	1.44
N_2	4.11	0.74	1.36
O_2	4.01	0.77	1.40

TABLE III. VSS parameters for unlike-species pairs ($T_{\text{ref}} = 273.15$ K).

Species pair (i-j)	$d_{\text{ref},i\text{-}j}$ (Å)	$\omega_{i\text{-}j}$	$\alpha_{i\text{-}j}$
He-Ar	3.205	0.725[a]	1.64[a]
N_2-O_2	4.06	0.755	1.38[a]
N_2-Ne	3.415	0.70	1.48[b]
N_2-Ar	4.11	0.775	1.33[a]
N_2-Kr	4.405	0.77	1.46[b]
N_2-Xe	4.88	0.795	1.58[b]

[a]Reference [32].

[b]The $\alpha_{N_2\text{-Ne}}$, $\alpha_{N_2\text{-Kr}}$, and $\alpha_{N_2\text{-Xe}}$ are calculated from the diffusion coefficient: $D_{\text{ref},N_2\text{-Ne}} = 0.2895 \times 10^{-4}$ m/s, $D_{\text{ref},N_2\text{-Kr}} = 0.1341 \times 10^{-4}$ m/s, and $D_{\text{ref},N_2\text{-Xe}} = 0.1108 \times 10^{-4}$ m/s [50].

and the mean collision time τ for the mixture is defined as the reciprocal of ν. The mean free path λ_i for each species i, as well as the overall mean free path λ of the mixture can be calculated as [32]

$$\lambda_i = \left\{ \sum_{j=1}^{s} \left[\pi (d_{\text{ref},i\text{-}j})^2 n_j (T_{\text{ref}}/T)^{\omega_{i-j}-0.5} \left(1 + \frac{m_i}{m_j}\right)^{0.5} \right] \right\}^{-1}, \tag{12}$$

$$\lambda = \sum_{i=1}^{s} \frac{n_i}{n} \lambda_i, \tag{13}$$

where m_i, m_j are the molecular mass for species i and j. Following Eq. (1), we can define the dimensionless parameter Y_i for each species i as

$$Y_i = \frac{L}{2\pi\lambda_i}, \tag{14}$$

and Y_m for the mixture can be obtained by substituting Eq. (13) into Eq. (1).

For mixtures including molecular gases such as N_2 and O_2, the modeling of inelastic collisions must be accounted for. Note that the temperature in all simulations of this work is below 800 K, so the vibrational energy excitation can be neglected [51] and only rotational-translational (RT) energy exchange is taken into account. At the macroscopic level, the RT energy exchange is popularly described via the Jeans equation [30,31]:

$$\frac{dT_{\text{rot},i}(t)}{dt} = \sum_{j=1}^{s} \frac{T_{tr,i}(t) - T_{\text{rot},i}(t)}{\tau_{\text{rot},i\text{-}j}} = \sum_{j=1}^{s} \frac{T_{tr,i}(t) - T_{\text{rot},i}(t)}{\tau_{i\text{-}j} Z_{i\text{-}j}}, \tag{15}$$

where $T_{tr,i}(t)$, $T_{\text{rot},i}(t)$ are the instantaneous translational and rotational temperatures of the species i; $\tau_{\text{rot},i\text{-}j}$ is the rotational relaxation time and can be further expressed as $\tau_{i\text{-}j} Z_{i\text{-}j}$, where $\tau_{i\text{-}j}$, $Z_{i\text{-}j}$ are the mean collision time and the rotational relaxation number of species i due to collisions with species j. Based on Eq. (15), we can further define a total rotational relaxation time $\tau_{\text{rot},i}$ for each species i in a gas mixture:

$$\frac{1}{\tau_{\text{rot},i}} = \frac{1}{\tau_i Z_{i,total}} = \sum_{j=1}^{s} \frac{1}{\tau_{i\text{-}j} Z_{i\text{-}j}}, \tag{16}$$

TABLE IV. Lennard-Jones potential parameters of the noble gas atoms [52].

Atom	ε_{ij}/k_B (K)	σ_{ij} (Å)
He	10.22	2.576
Ne	35.7	2.789
Ar	124	3.418
Kr	190	3.610
Xe	229	4.055

where $\tau_i = \frac{1}{\nu_i}$ is the mean collision time for species i in a gas mixture; $Z_{i,total}$ denotes the total rotational relaxation number of species i.

For DSMC simulations of molecular gas mixtures, the BL model [41] is employed in this work to distribute the post-collision energy between translational and rotational modes of each selected pair for inelastic collisions, to match the Jeans equation [Eq. (15)] at the macroscopic level. Besides, the pair selection method proposed by Haas *et al.* [30] is used to determine the inelastic collision probability $P_{i\text{-}j}$, which is directly related to the rotational relaxation number $Z_{i\text{-}j}$ as [30]

$$Z_{i\text{-}j} = \left[P_{i\text{-}j}(1 - 0.5P_{j\text{-}i}) \frac{\hat{d}_{T,i\text{-}j}}{\hat{d}_{T,i\text{-}j} + \hat{d}_{r,i}} \right]^{-1}, \tag{17}$$

where $\hat{d}_{T,i\text{-}j} = 5\text{-}2\omega_{i\text{-}j}$ is the translational degrees of freedom of the colliding species pair i–j, and $\hat{d}_{r,i}$ is the rotational degrees of freedom of species i. Therefore, determining each probability $P_{i\text{-}j}$ in DSMC is equivalent to determining each rotational relaxation number $Z_{i\text{-}j}$ in Eq. (15). In the following we use $Z_{i\text{-}j}$ for simplicity.

All the DSMC simulations are performed in the freely distributed code SPARTA [37]. To ensure the simulation accuracy, the calculation time step is equal to 0.1τ, and the cell length in the y direction is smaller than $\frac{1}{3}\lambda$. For calculations involving molecular gases, all of the $Z_{i\text{-}j}$ are assumed to be constant, and they are determined by fitting the RBS spectra obtained by DSMC with the ones determined by MD.

B. Molecular dynamics method

The MD method uses interatomic potentials instead of phenomenological models to describe the interatomic interactions. Once the PESs of the system are determined, the RBS spectra calculated by MD can be compared to the experiments without any fitting parameters. In this work, the Lennard-Jones (LJ) potential [52] is used to describe the interactions between atoms,

$$u(r_{ij}) = \begin{cases} 4\varepsilon_{ij}\left[\left(\frac{\sigma_{ij}}{r_{ij}}\right)^{12} - \left(\frac{\sigma_{ij}}{r_{ij}}\right)^{6}\right], & r_{ij} \leqslant r_{\text{cutoff}}, \\ 0, & r_{ij} > r_{\text{cutoff}} \end{cases} \tag{18}$$

where r_{ij} is the distance between two interacting atoms i and j, ε_{ij} is the potential well depth, σ_{ij} denotes the distance at which the potential $u(r_{ij})$ is zero, and r_{cutoff} is the potential cutoff distance. The LJ potential parameters for different noble gas atoms are shown in Table IV [52].

For molecular gases such as N_2 and O_2, they are modeled as rigid rotors with no vibrational excitation.

TABLE V. Two-site Lennard-Jones potential parameters of the molecular gas atoms.

Atom	ε_{ij}/k_B (K)	σ_{ij} (Å)
N	47.2[a]	3.17[a]
O	48.0[b]	3.006[b]

[a]Reference [42].
[b]Reference [53].

The interatomic bond lengths are fixed as their equilibrium bond lengths, that is, 1.097 Å [42] and 1.208 Å [53] for N_2 and O_2, respectively. To calculate intermolecular interaction, Eq. (18) is also used [42,53] between atom i of molecule 1 and atom j of molecule 2. The potential parameters for N_2 and O_2 are shown in Table V [42,53].

For gas mixtures, the widely used Lorentz–Berthelot combining rules are employed to describe the cross interactions [36]:

$$\varepsilon_{ab} = \sqrt{\varepsilon_{aa}\varepsilon_{bb}}, \tag{19}$$

$$\sigma_{ab} = \frac{\sigma_{aa} + \sigma_{bb}}{2}. \tag{20}$$

For all the simulations, the r_{cutoff} is set to be 12 Å.

The MD simulations are performed in the freely distributed code LAMMPS [54]. All the cases are run in a microcanonical (*NVE*) ensemble, where the total energy, density, and volume of the system remain constant. The simulation time step is set as 5 fs if not specifically indicated.

IV. RESULTS AND DISCUSSIONS

In this section, we calculate the RBS spectra of different kinds of gas mixtures following the methods proposed in Sec. III. After the original calculated RBS spectra are obtained, they are convoluted with the instrument function provided in Refs. [22,28]. For the sake of comparison between the calculated RBS spectra in this work and the experimental spectra in the literature, they are normalized to ensure the integral of the spectrum over the entire frequency range is equal to 1. The relative residuals between MD spectra and experimental spectra are estimated as

$$\tilde{R}_{\text{expt-MD}}(f_i) = \frac{S_{\text{expt}}(f_i) - S_{\text{MD}}(f_i)}{\max(S_{\text{MD}})}, \tag{21}$$

where f_i represents the discrete frequency point, S_{expt} and S_{MD} represent the RBS spectra of experiments and MD calculations, and $\max(S_{\text{MD}})$ denotes the maximum value of the MD result. Similarly, the relative residuals between DSMC spectra and MD spectra can be calculated as

$$\tilde{R}_{\text{DSMC-MD}}(f_i) = \frac{S_{\text{DSMC}}(f_i) - S_{\text{MD}}(f_i)}{\max(S_{\text{MD}})}, \tag{22}$$

where S_{DSMC} denotes the RBS spectrum calculated by the DSMC method.

TABLE VI. The simulation conditions for Ar-He mixtures. All the simulations are performed at $T = 297$ K and $L = 284.96$ nm.

P_{Ar} (bar)	P_{He} (bar)	Y_{Ar}	Y_{He}	Y_m
2	—	1.62	—	1.62
1	3	4.29	1.14	1.39
2	2	3.94	1.25	1.90
3	1	3.59	1.36	2.54

A. Argon-helium gas mixtures

In this subsection, we calculate the RBS spectra for mixtures of Ar and He, which have been studied by Gu *et al.* [28] using kinetic model equations and Bruno *et al.* [40] using the DSMC method. In the present work, we study them using the MD method; therefore, we first validate the use of the MD method by comparing its results with those obtained by experiments [28]. Then, we calculate the RBS spectra using the DSMC method under the same conditions. By comparing DSMC and MD results, we can verify the consistency of these two methods. It is worth noting that, since the mixtures do not contain polyatomic molecules, there is no need to adjust any parameters in the DSMC simulations.

The simulation conditions are shown in Table VI, which correspond to the experimental conditions of Gu *et al.* [28]. We calculate three mixture conditions by changing the partial pressure P_i of each component while keeping the total pressure of the mixture constant. Besides, the RBS spectrum of Ar at $P_{\text{Ar}} = 2$ bars is calculated for the follow-up discussions. All the simulations are performed at $T = 297$ K and $L = 284.96$ nm. Following Eqs. (1) and (14), we obtain the dimensionless parameters Y_{Ar}, Y_{He}, and Y_m for different conditions, which are also presented in Table VI.

For both DSMC and MD simulations, the average number of simulated molecules in each space bin is more than 25 for each species. Besides, for MD simulations including He atoms, as the weight of the He atom is much lighter than other types of molecules (see Table I), the time step is reduced to 2 fs to ensure the simulation accuracy. The instrument function provided in Ref. [28] is used for the convolution process.

Figure 4 shows the comparison of MD calculated spectra and experimental spectra under the conditions presented in Table VI. It can be seen that the RBS spectra calculated by MD agree well with the experimental spectra under all conditions. In most cases, the relative residuals between MD spectra and experimental spectra are below 3%, except for the case of $P_{\text{Ar}} = 2$ bars and $P_{\text{He}} = 2$ bars, where the maximum residual is around 5%. We further compare the MD calculated spectrum with that calculated by the kinetic model equations [28]. As shown in Fig. 4(g), the relative residuals between the MD spectrum and the kinetic model spectrum are much smaller, indicating that there might be non-negligible errors in the experiments. The aforementioned comparisons demonstrate that as long as the PESs of the gas mixtures are correctly provided, the RBS spectrum determined by MD can be regarded as a standard, and it can be further used to evaluate the accuracy of the DSMC results.

Figure 5 shows the RBS spectra obtained by DSMC and MD methods under the same conditions given in Table VI.

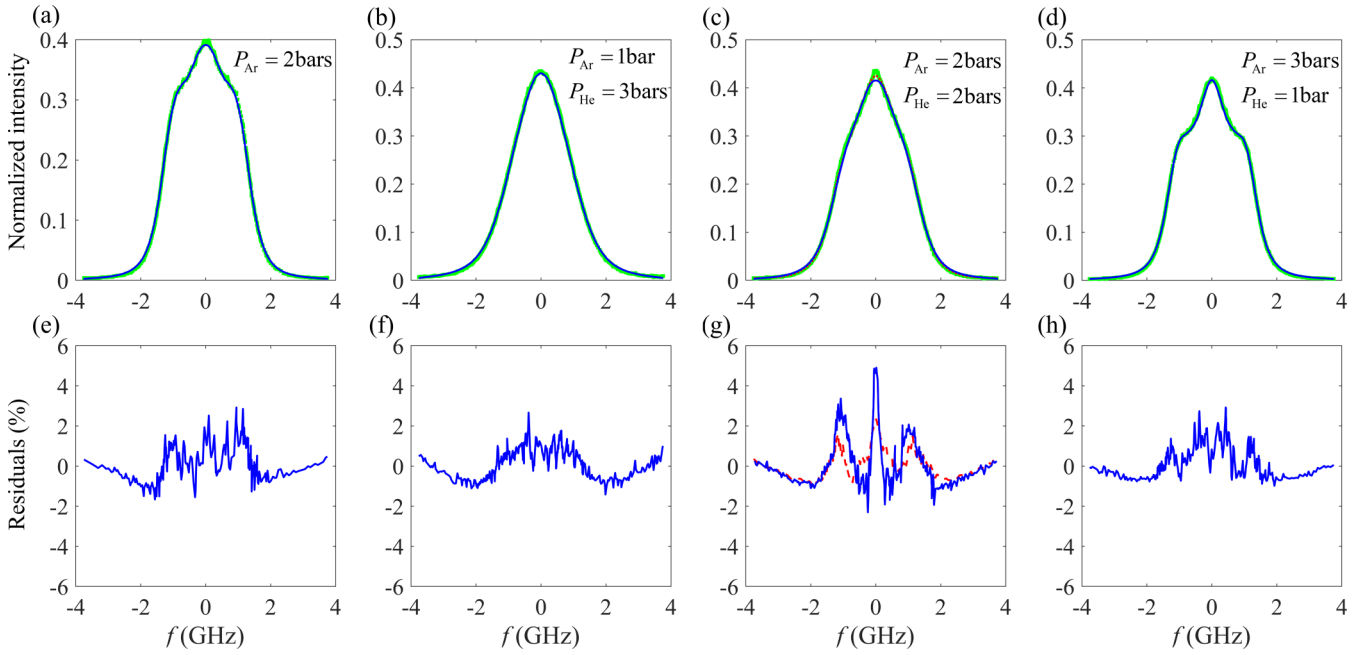

FIG. 4. Panels (a–d) show the comparison of MD calculated RBS spectra (blue solid line) with those measured from the experiments [28] (green square) under conditions presented in Table VI, and panels (e–h) show the corresponding residuals (solid line). Panel (c) also displays the RBS spectrum calculated by kinetic model equations [28] (red dotted line), and the residuals between kinetic model and MD results (dashed line) are shown in panel (g).

It can be seen that the RBS spectra calculated by DSMC agree well with those calculated by the MD method. We also calculate the relative residuals between spectra calculated by the two methods, which are less than 1% for all the conditions. This indicates that our DSMC and MD simulations can predict almost the same properties of Ar-He gas mixtures.

It is interesting to compare the RBS line shapes in Figs. 5(a) and 5(c), where the pressure of Ar remains constant but the pressure of He is different. It is shown that although the mass and polarizability of He atoms are much lower than those of Ar atoms (see Table I), their existence can still change the shape of the RBS spectrum to a large extent. This conclusion is similar to those reported by Refs. [28,40]. In addition, it can be seen from Figs. 5(b)–5(d) that the RBS spectra have more obvious Brillouin peaks as P_{Ar} increases. The reason for this is that increasing P_{Ar} is equivalent to increasing Y_m, as shown in Table VI.

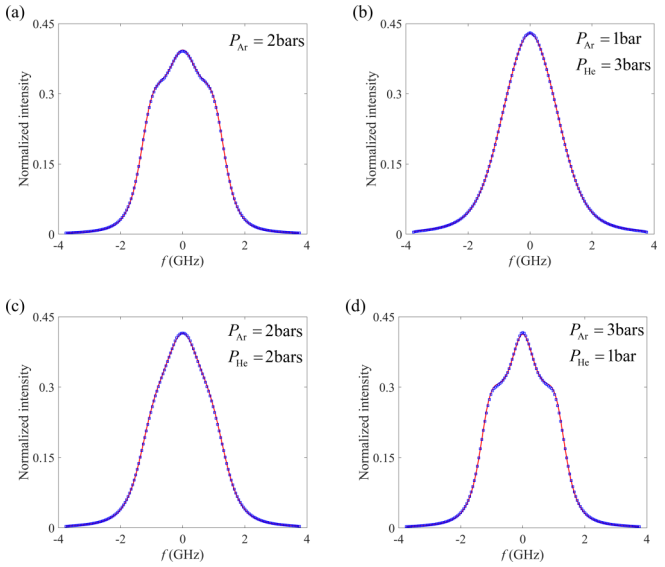

FIG. 5. Comparison of DSMC (line) and MD (square) spectra under conditions given in Table VI.

B. Air

We then extend our MD and DSMC calculations to air. It is worth noting that the previous studies using the Tenti S6 model considered air as a single-component gas with effective gas parameters [16,22,47]. In the present study, air is instead assumed to be a mixture of N_2 (78.85%) and O_2 (21.15%).

The simulation conditions are shown in Table VII, which can be divided into three groups. The first group corresponds

TABLE VII. The simulation conditions of N_2, O_2, and air. All the simulations are performed at $P = 3$ bars.

Condition group	Gas	T (K)	L (nm)	Y_m
Group 1	N_2	297.3	285	2.44
	O_2	297.6	285	2.31
	air	296.8	283.7	2.41
Group 2	N_2	500	532	2.39
	O_2	500	532	2.23
	air	500	532	2.36
Group 3	N_2	750	884.6	2.40
	O_2	750	884.6	2.22
	air	750	884.6	2.36

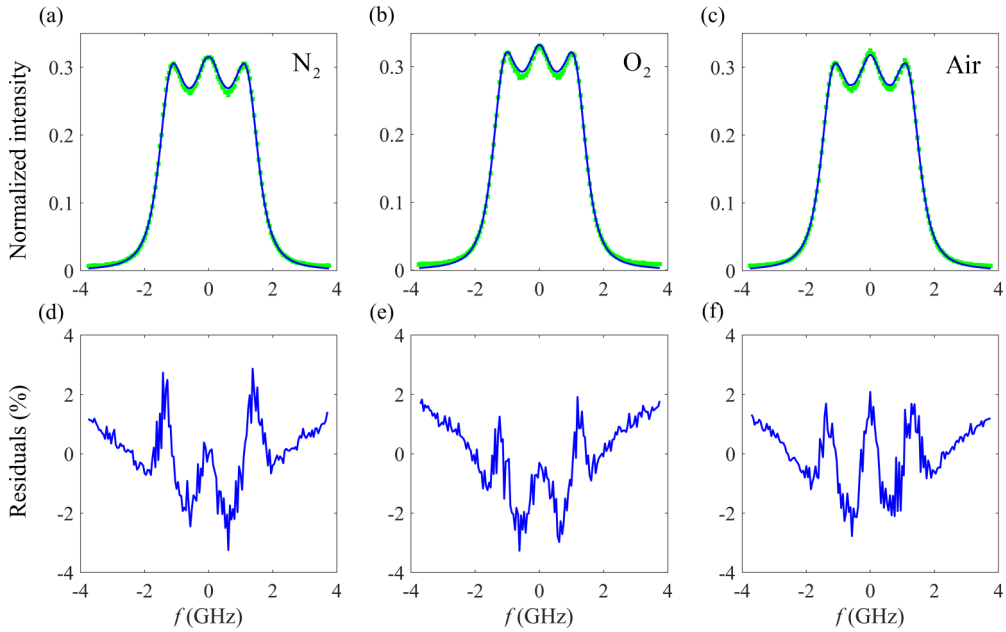

FIG. 6. Panels (a–c) show the comparison of MD calculated RBS spectra (line) with those measured from the experiments [22] (square) for the first group of conditions presented in Table VII, and panels (d–f) show the corresponding residuals.

to the experimental conditions of Gu and Ubachs [22], and the other groups have the simulated temperatures higher than the experimental temperature range. For comparison, we also calculate RBS spectra of pure N_2 and O_2 under the same temperature conditions besides air. Since the mean free path of the gas increases with increasing temperature, we choose a longer L at a higher temperature to keep the Y_m value around 2.33 ($\pm$0.11). All the simulations are performed at $P = 3$ bars. The instrument function provided in Ref. [22] is employed for the convolution process.

To verify the accuracy of MD calculations, we first compare the MD spectra to the experimental spectra under the first group of conditions (see Table VII). As can be seen from Fig. 6, the RBS spectra of N_2, O_2, and air calculated by MD are in good agreement with those obtained from experiments. In all the cases, the maximum residual between MD and experimental spectra is around 3%. The comparisons validate the applicability of MD potential parameters given in Table V.

For DSMC simulations, there are four rotational relaxation numbers that need to be accounted for, that is, $Z_{N_2\text{-}N_2}$, $Z_{O_2\text{-}O_2}$, $Z_{N_2\text{-}O_2}$, and $Z_{O_2\text{-}N_2}$. Specifically, $Z_{N_2\text{-}N_2}$ and $Z_{O_2\text{-}O_2}$ correspond to the rotational relaxation numbers of the like-species pairs, while $Z_{N_2\text{-}O_2}$ is the rotational relaxation number of N_2 due to collisions with O_2, and $Z_{O_2\text{-}N_2}$ is the rotational relaxation number of O_2 due to collisions with N_2. Using the inelastic pair selection method [30] introduced in Sec. III A, these four relaxation numbers can be set separately in DSMC simulations, and their specific values are determined by fitting the RBS spectra obtained by DSMC to the MD results. The relative error between DSMC and MD spectra can be evaluated using the normalized root-mean-square deviation (D_{rms}) defined as

$$D_{\text{rms}} = \frac{\sqrt{\frac{1}{N}\sum_{i=1}^{N}\left[S_{\text{DSMC}}(f_i) - S_{\text{MD}}(f_i)\right]^2}}{\max(S_{\text{MD}})}, \tag{23}$$

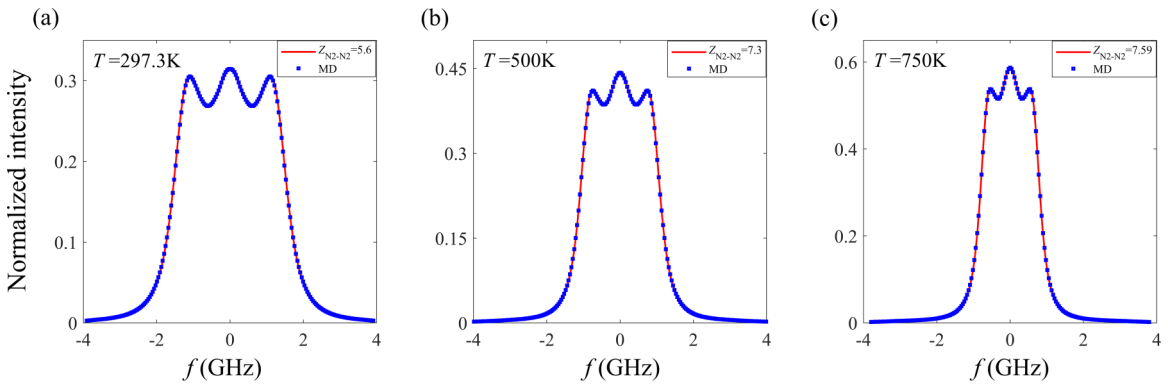

FIG. 7. Comparison of DSMC and MD spectra for N_2 at (a) $T = 297.3$ K, (b) $T = 500$ K, and (c) $T = 750$ K. The DSMC spectra correspond to the best fitting values of $Z_{N_2\text{-}N_2}$.

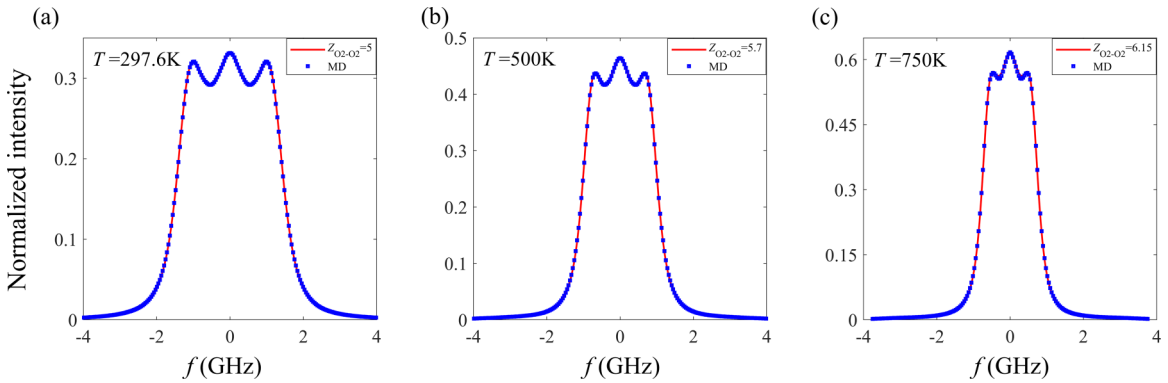

FIG. 8. Comparison of DSMC and MD spectra for O_2 at (a) $T = 297.6$ K, (b) $T = 500$ K, and (c) $T = 750$ K. The DSMC spectra correspond to the best fitting values of $Z_{O_2\text{-}O_2}$.

where N is the number of discrete frequency points. Therefore, the best fitting between DSMC and MD spectra is found at the lowest D_{rms} value.

Due to the complexity of determining four rotational relaxation numbers simultaneously, we first determine the values of $Z_{N_2\text{-}N_2}$ and $Z_{O_2\text{-}O_2}$ by fitting the DSMC spectra of N_2 and O_2 to the corresponding MD results. After the values of $Z_{N_2\text{-}N_2}$ and $Z_{O_2\text{-}O_2}$ are extracted, they can be directly used in the DSMC simulations of air. The results in Figs. 7 and 8 show that the DSMC spectra agree well with MD spectra under all the conditions. We also calculate the relative residuals between spectra calculated by the two methods, which are less than 1.3% for all the conditions.

To validate the $Z_{N_2\text{-}N_2}$ and $Z_{O_2\text{-}O_2}$ determined by the aforementioned calculations, in Fig. 9 we compare them to the ones obtained with the Parker model [55,56]. In addition, in Fig. 9(a) we also compare our $Z_{N_2\text{-}N_2}$ results to those obtained by Valentini *et al.* [42] using MD simulations. Based on the Jeans equation [Eq. (15)] for the case of one-component gas, we achieve the comparison of different methods following the rules below [31]:

$$Z^{\text{DSMC}}\tau^{\text{DSMC}} = Z^{\text{others}}\tau^{\text{others}}, \tag{24}$$

where Z^{DSMC} and τ^{DSMC} are the rotational relaxation number and the mean collision time defined in our DSMC simulations, while Z^{others} and τ^{others} are the ones defined in other methods. In Fig. 9, the relaxation numbers obtained by different methods are compared under the same definition of τ as [55,56]

$$\tau = \frac{\pi\mu_s}{4P}. \tag{25}$$

As can be seen from Fig. 9(a), the $Z_{N_2\text{-}N_2}$ values we determine lie among the ones obtained by other methods. As can be seen from Fig. 9(b), at a lower temperature of 297.6 K, the $Z_{O_2\text{-}O_2}$ we obtain is closer to the one obtained by Lordi and Mates [56], while at higher temperatures, the results we get are closer to the ones obtained by Parker [55]. In general, the results show that, by fitting the DSMC spectra to the MD spectra, one can obtain the rotational relaxation numbers of one-component gases which are close to the previous studies.

After $Z_{N_2\text{-}N_2}$ and $Z_{O_2\text{-}O_2}$ are well determined, we then calculate the RBS spectra of air under the same temperature conditions. For the determination of $Z_{N_2\text{-}O_2}$ and $Z_{O_2\text{-}N_2}$, based on the similarity between N_2 and O_2 molecules, in this paper

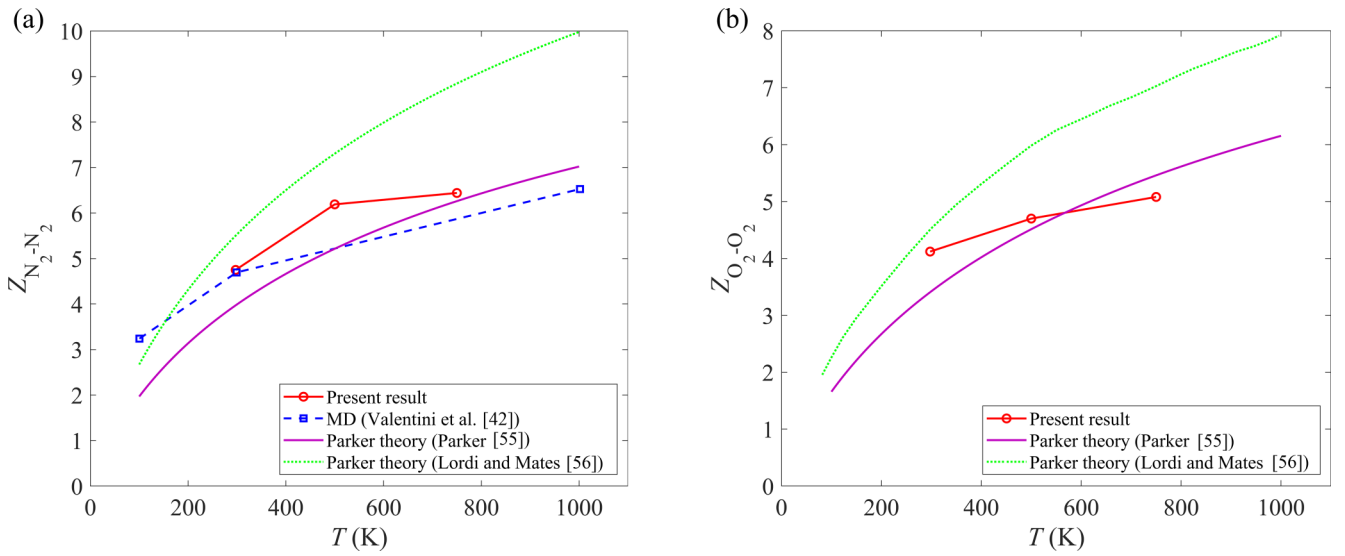

FIG. 9. The equilibrium rotational relaxation numbers $Z_{N_2\text{-}N_2}$ (a) and $Z_{O_2\text{-}O_2}$ (b) obtained from RBS calculations.

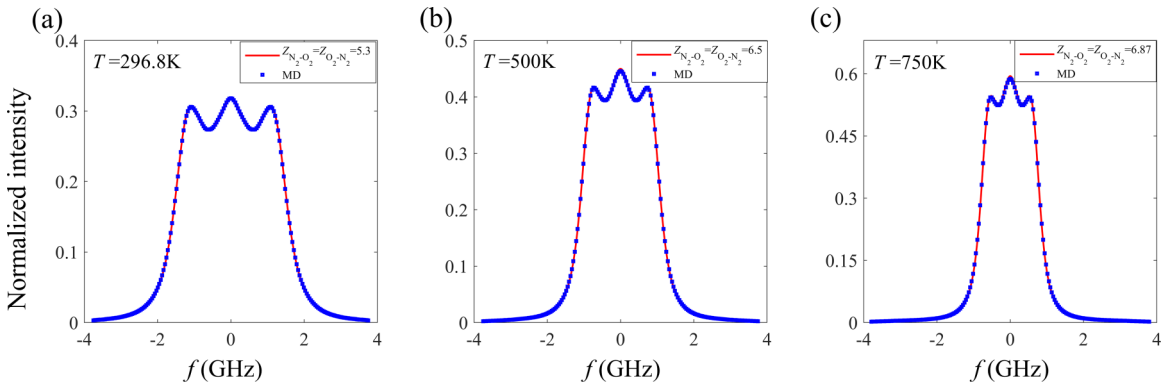

FIG. 10. Comparison of DSMC and MD spectra for air at (a) $T = 296.8$ K, (b) $T = 500$ K, and (c) $T = 750$ K.

we assume they have the same value as

$$Z_{\mathrm{N_2\text{-}O_2}} = Z_{\mathrm{O_2\text{-}N_2}} = \tfrac{1}{2}\left(Z_{\mathrm{O_2\text{-}O_2}} + Z_{\mathrm{N_2\text{-}N_2}}\right), \tag{26}$$

and this assumption will be validated by comparing the DSMC spectra of air to the ones calculated by the MD method.

As shown in Fig. 10, the DSMC spectra are in good agreement with the MD spectra under all the simulation conditions. At $T = 296.8$ K, the maximum residual between DSMC and MD spectra is around 0.5%, while at a higher temperature, this value increases to around 1%. The results show that it is quite reasonable to use Eq. (26) to approximate both $Z_{\mathrm{N_2\text{-}O_2}}$ and $Z_{\mathrm{O_2\text{-}N_2}}$ in the DSMC simulations of air. The $Z_{\mathrm{N_2\text{-}N_2}}$, $Z_{\mathrm{O_2\text{-}O_2}}$, $Z_{\mathrm{N_2\text{-}O_2}}$, and $Z_{\mathrm{O_2\text{-}N_2}}$ we obtained are shown in Fig. 11(a), which indicates that all the rotational relaxation numbers increase as the temperature rises. The obtained rotational relaxation numbers can be used for the DSMC simulations of air under the near-equilibrium conditions.

Based on the extracted rotational relaxation numbers, the bulk viscosities μ_b of N_2, O_2, and air can be further estimated. For N_2 and O_2, the μ_b can be calculated as [24,57,58]

$$\mu_b = \frac{PR}{{c_v}^2} c_{v,\mathrm{int}} \tau_{\mathrm{rot}} = \frac{4}{25} P \tau_{\mathrm{rot}}, \tag{27}$$

where R is the specific gas constant, $c_{v,\mathrm{int}} = \frac{\hat{d}_r}{2} R = R$ is the isochoric internal specific heat, $c_v = \frac{3+\hat{d}_r}{2} R = \frac{5}{2} R$ is the total isochoric specific heat, and $\tau_{\mathrm{rot}}{=}Z\tau$ is the rotational relaxation time. For air, Eq. (27) can also be used, but τ_{rot} now denotes the overall relaxation time for the mixture, which can be expressed as [57,58]

$$\tau_{\mathrm{rot}} = \sum_{i=1}^{s} x_i (c_{v,\mathrm{int},i}/c_{v,\mathrm{int}}) \tau_{\mathrm{rot},i}, \tag{28}$$

where x_i denotes the mole fraction of the species i, and $c_{v,\mathrm{int},i}$ denotes the isochoric internal specific heat of the species i. $\tau_{\mathrm{rot},i}$ can be further calculated by the fitted rotational relaxation numbers [see Eq. (16)]. Finally, the results of μ_b that we obtained are shown in Fig. 11(b).

C. Nitrogen-noble gas mixtures

In this subsection, we further extend our research to the binary gas mixtures composed of N_2 and one noble monatomic gas. For this type of gas mixtures, previous studies using theoretical analysis [59], classical trajectory (CT) calculations [60], and acoustical absorption measurements [60,61] mainly focus on how the rotational energy relaxation of N_2 is affected

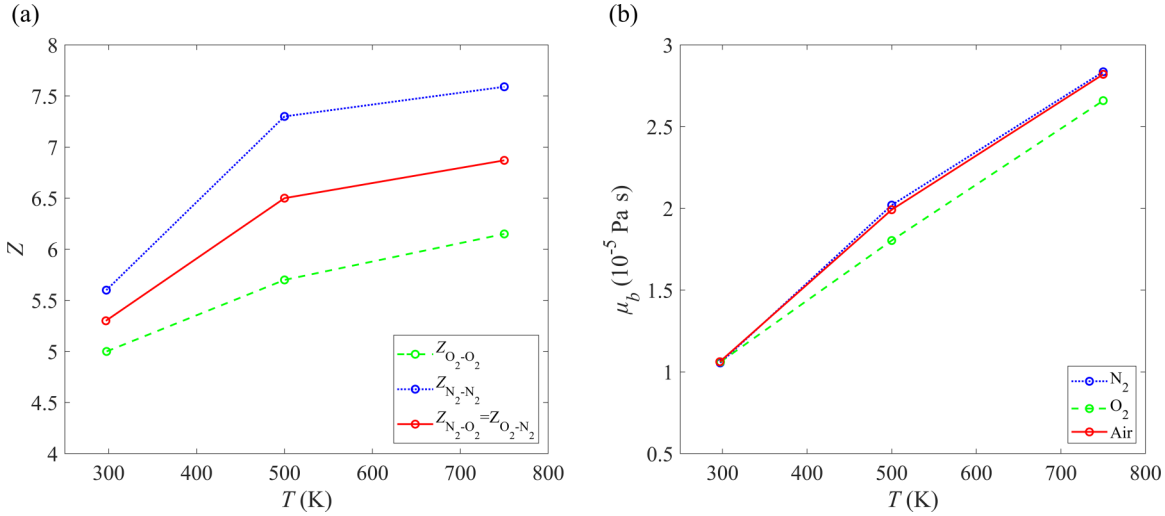

FIG. 11. (a) The $Z_{\mathrm{N_2\text{-}N_2}}$, $Z_{\mathrm{O_2\text{-}O_2}}$, $Z_{\mathrm{N_2\text{-}O_2}}$, and $Z_{\mathrm{O_2\text{-}N_2}}$ obtained from the RBS calculations. (b) The μ_b of N_2, O_2, and air calculated from the rotational relaxation numbers.

TABLE VIII. The simulation conditions of N_2−x mixtures. All the simulations are performed at $T = 297.3$ K and $L = 284.96$ nm.

N_2−x	P_{N_2} (bar)	P_x (bar)	Y_{N_2}	Y_x	Y_m
N_2-Ne	3	3	4.28	2.64	3.27
N_2-Ar	2	1	2.37	2.59	2.44
N_2-Kr	2	1	2.39	3.69	2.70
N_2-Xe	3	1.5	3.77	8.05	4.58

by noble gas atoms with different masses. Here we propose to study this effect through RBS calculations.

The simulation conditions are shown in Table VIII. For convenience of discussion, we use N_2−x to represent the mixture of N_2 and a kind of noble gas x. The scattering wavelength L we choose for all the simulations is equal to 284.96 nm. All the simulations are performed at $T = 297.3$ K, under which $Z_{N_2\text{-}N_2}$ has been determined by RBS calculations for N_2 [see Fig. 7(a)]. Therefore, for all the DSMC calculations, we set the value of $Z_{N_2\text{-}N_2}$ equal to 5.6, while the values of $Z_{N_2\text{-}x}$ are determined by fitting the DSMC calculated spectra to the corresponding MD results.

To reduce the difficulty of determining $Z_{N_2\text{-}x}$, we choose the appropriate simulated pressure for each condition to ensure that the Brillouin peaks in the RBS spectra can be clearly distinguished. Additionally, the partial pressure of each component is set to ensure that there are enough collisions between N_2 and x molecules, so that the influence of $Z_{N_2\text{-}x}$ on the RBS spectrum is significant. The instrument function provided in Ref. [22] is employed for the convolution process.

Figures 12 and 13 show the RBS spectra calculated by DSMC and MD under the four simulation conditions shown in Table VIII. It can be seen that decreasing the value of $Z_{N_2\text{-}x}$ increases the intensity of the Brillouin peaks, which is similar to the case of one-component gas [39]. For N_2-Ne and N_2-Ar mixtures, by fitting the DSMC spectra to the MD spectra we can obtain $Z_{N_2\text{-Ne}} = 17.5(\pm 2.0)$ and $Z_{N_2\text{-Ar}} = 7.1\ (\pm 1.4)$. As can be seen from Fig. 12, the DSMC spectra agree well with MD spectra, and the maximum residual between them is around 0.5%.

For N_2-Kr and N_2-Xe gas mixtures, the relative errors between DSMC and MD spectra are increased compared to those of N_2-Ne and N_2-Ar mixtures, as shown in Fig. 13, and these errors cannot be eliminated by only adjusting $Z_{N_2\text{-}x}$ in DSMC simulations. It indicates that accurate DSMC calculations of N_2-Kr and N_2-Xe gas mixtures may require more complex molecular interaction models, and this is beyond the scope of this work. Here we determine a relatively optimal $Z_{N_2\text{-}x}$ at a low D_{rms} value between MD and DSMC spectra. The determined values of $Z_{N_2\text{-Kr}}$ and $Z_{N_2\text{-Xe}}$ are 7.7 (± 1.1) and 15.9 (± 2.1), respectively, and the maximum residual between DSMC and MD spectra is around 1%.

Based on the aforementioned RBS calculations, the effect of the noble gas atoms on the rotational relaxation process of N_2 is studied. Figure 14 shows that as m_x/m_{N_2} increases, the $Z_{N_2\text{-}x}$ decreases first and then increases. The minimum value of $Z_{N_2\text{-}x}$ is 7.1 for $Z_{N_2\text{-Ar}}$, corresponding to m_x/m_{N_2} of 1.43. This phenomenon can be qualitatively explained as follows: The $Z_{N_2\text{-}x}$ represents the average number of collisions required for a N_2 molecule to reach rotational energy equilibrium due to collisions with species x atoms. When the gas temperature

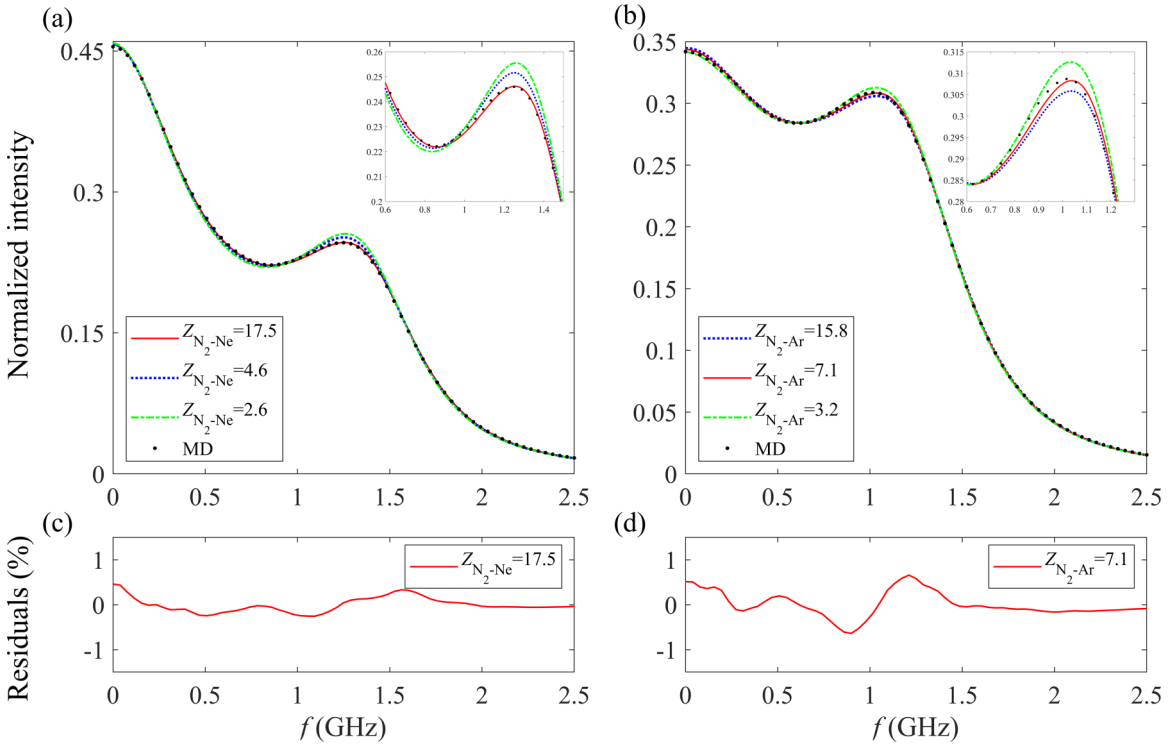

FIG. 12. Comparison of DSMC and MD spectra for the N_2-Ne (a) and N_2-Ar (b) gas mixtures. Panels (c,d) show the corresponding residuals for the best fitting values of $Z_{N_2\text{-}x}$.

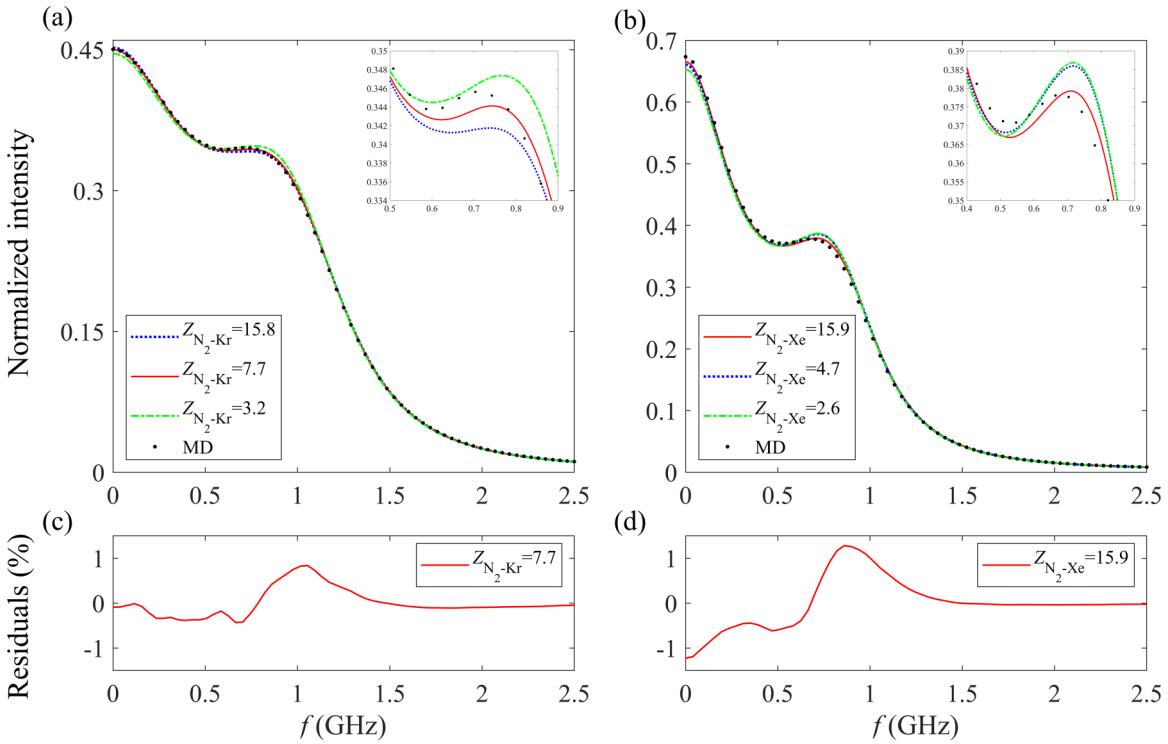

FIG. 13. Comparison of DSMC and MD spectra for the N_2-Kr (a) and N_2-Xe (b) gas mixtures. Panels (c,d) show the corresponding residuals for the best fitting values of $Z_{N_2\text{-}x}$.

stays constant, the average thermal motion momentum of an atom increases as its mass increases, resulting in a greater impact on the movement of N_2 molecules and hence causing them to reach rotational energy equilibrium with a smaller number of collisions. Therefore, $Z_{N_2\text{-}x}$ initially decreases as the m_x increases. However, as m_x exceeds a certain value, the atom's momentum is so large that one collision is more likely to make one N_2 molecule jump from one nonequilibrium state to another, instead of reaching equilibrium state. In this case, N_2 molecules conversely need more collisions to reach the rotational energy equilibrium, corresponding to a larger $Z_{N_2\text{-}x}$. It is worth noting that this phenomenon was also reported

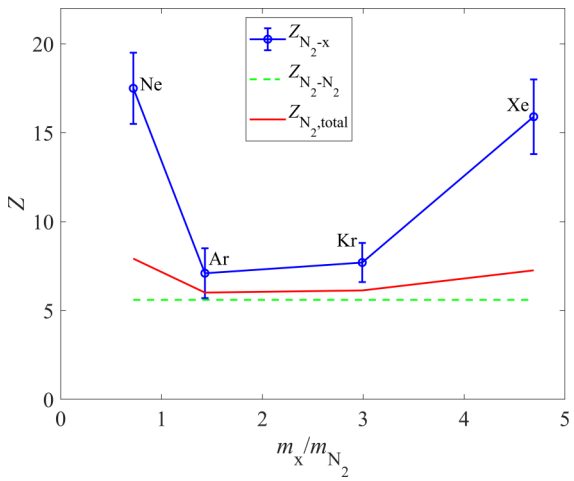

FIG. 14. The changes of $Z_{N_2\text{-}x}$, $Z_{N_2-N_2}$, and $Z_{N_2,\text{total}}$ against the mass ratio between species x and N_2. The error bars of the obtained $Z_{N_2\text{-}x}$ are also displayed.

by Kistemaker and Vries [60] using acoustical absorption measurements and CT calculations, although their results gave a smaller m_x/m_{N_2} value for the minimum value of $Z_{N_2\text{-}x}$.

According to Eq. (16), we further obtain the total rotational relaxation number $Z_{N_2,\text{total}}$ for N_2 in mixtures as

$$Z_{N_2,\text{total}} = \left[\tau_{N_2}\left(\frac{1}{\tau_{N_2\text{-}N_2}Z_{N_2\text{-}N_2}} + \frac{1}{\tau_{N_2\text{-}x}Z_{N_2\text{-}x}}\right)\right]^{-1}, \quad (29)$$

where τ_{N_2} is the mean collision time of N_2 in the N_2–x mixture. As can be seen from Fig. 14, the values of $Z_{N_2,\text{total}}$ are obviously larger than those of the $Z_{N_2\text{-}N_2}$, which means that the presence of the noble gas atoms slows down the total rotational relaxation rate of N_2, compared to one-component N_2 gas.

V. CONCLUSION

In this work, we employ two widely used molecular simulation methods, i.e., DSMC and MD, to study the spontaneous RBS in binary gas mixtures. The two methods are first validated by comparing the calculated spectra of Ar-He gas mixtures to the corresponding experimental results. Then, we successfully extend our calculations to mixtures involving molecular gases. By considering MD calculated spectra as standards, we extract the rotational relaxation numbers $Z_{i\text{-}j}$ specific to each species pair i-j by fitting the DSMC spectra to MD spectra.

Our calculation results show that, for a mixture of N_2 and O_2, the four rotational relaxation numbers, i.e., $Z_{N_2\text{-}N_2}$, $Z_{O_2\text{-}O_2}$, $Z_{N_2\text{-}O_2}$, and $Z_{O_2\text{-}N_2}$, increase with temperature in the range of 300–750 K, and the values of $Z_{N_2\text{-}O_2}$ and $Z_{O_2\text{-}N_2}$ can be assumed to be equal to the average of $Z_{N_2\text{-}N_2}$ and $Z_{O_2\text{-}O_2}$.

We further calculate the RBS spectra for binary gas mixtures composed of N_2 and one noble monatomic gas x (Ne, Ar, Kr, Xe) at $T = 297.3$ K. The calculation results show that as the atomic mass of species x increases, the $Z_{N_2\text{-}x}$ first decreases and then increases, and it reaches the minimum value of 7.1 for the case of the N_2-Ar mixture. Besides, the total rotational relaxation number $Z_{N_2,\text{total}}$ is obviously greater than $Z_{N_2\text{-}N_2}$, which means that the presence of the noble gas atoms will slow down the rotational relaxation of N_2, compared to the case of one-component N_2 gas.

Our results demonstrate that the molecular simulation approaches can obtain the RBS spectra of complex gas mixtures with high accuracy. Meanwhile, the calculation of RBS spectra can provide a promising and alternative way to study the rotational relaxation process in gas mixtures.

ACKNOWLEDGMENTS

We thank Lei Wu, Wilson Marques, Jr., and Yuanqing Wang for their help in light scattering theory, and Ziyu Gu for providing the experimental results. This work was supported by the National Natural Science Foundation of China (Grants No. 92052104 and No. 11772034). Results were obtained using the Tianhe-2 supercomputer.

[1] B. Witschas, C. Lemmerz, and O. Reitebuch, Daytime measurements of atmospheric temperature profiles (2–15 km) by lidar utilizing Rayleigh-Brillouin scattering, Opt. Lett. **39**, 1972 (2014).

[2] O. Reitebuch, C. Lemmerz, E. Nagel, U. Paffrath, Y. Durand, M. Endemann, F. Fabre, and M. Chaloupy, The airborne demonstrator for the direct-detection Doppler wind Lidar ALADIN on ADM-Aeolus. Part I: Instrument design and comparison to satellite instrument, J. Atmos. Oceanic Technol. **26**, 2501 (2009).

[3] X. Zhai, U. Marksteiner, F. Weiler, C. Lemmerz, O. Lux, B. Witschas, and O. Reitebuch, Rayleigh wind retrieval for the ALADIN airborne demonstrator of the Aeolus mission using simulated response calibration, Atmos. Meas. Tech. **13**, 445 (2020).

[4] R. B. Miles, W. R. Lempert, and J. N. Forkey, Laser Rayleigh scattering, Meas. Sci. Technol. **12**, R33 (2001).

[5] M. Boguszko and G. S. Elliott, On the use of filtered Rayleigh scattering for measurements in compressible flows and thermal fields, Exp. Fluids **38**, 33 (2004).

[6] Z. Gu, Ph.D. thesis, Spontaneous Rayleigh-Brillouin scattering on atmospheric gases, Vrije Universiteit Amsterdam, 2015.

[7] Y. Wang, W. Ubachs, and W. van de Water, Bulk viscosity of CO_2 from Rayleigh-Brillouin light scattering spectroscopy at 532 nm, J. Chem. Phys. **150**, 154502 (2019).

[8] L. Wu, Q. Li, H. Liu, and W. Ubachs, Extraction of the translational Eucken factor from light scattering by molecular gas, J. Fluid Mech. **901**, A23 (2020).

[9] Y. Wang, Ph.D. thesis, Spontaneous Rayleigh-Brillouin scattering in molecular gases, Vrije Universiteit Amsterdam, 2019.

[10] J. Zhang and J. Fan, Monte Carlo simulation of thermal fluctuations below the onset of Rayleigh-Bénard convection, Phys. Rev. E **79**, 056302 (2009).

[11] J. H. Grinstead and P. F. Barker, Coherent Rayleigh Scattering, Phys. Rev. Lett. **85**, 1222 (2000).

[12] X. Pan, M. N. Shneider, and R. B. Miles, Coherent Rayleigh-Brillouin Scattering, Phys. Rev. Lett. **89**, 183001 (2002).

[13] J. P. Boon and S. Yip, *Molecular Hydrodynamics* (McGraw-Hill, New York, 1980).

[14] B. J. Berne and R. Pecora, *Dynamic Light Scattering* (Wiley, New York, 1976).

[15] M. O. Vieitez, E. J. van Duijn, W. Ubachs, B. Witschas, A. Meijer, A. S. de Wijn, N. J. Dam, and W. van de Water, Coherent and spontaneous Rayleigh-Brillouin scattering in atomic and molecular gases and gas mixtures, Phys. Rev. A **82**, 043836 (2010).

[16] B. Witschas, Z. Gu, and W. Ubachs, Temperature retrieval from Rayleigh-Brillouin scattering profiles measured in air, Opt. Express **22**, 29655 (2014).

[17] S. Yip and M. Nelkin, Application of a kinetic model to time-dependent density correlations in fluids, Phys. Rev. **135**, A1241 (1964).

[18] A. Sugawara, S. Yip, and L. Sirovich, Spectrum of density fluctuations in gases, Phys. Fluids **11**, 925 (1968).

[19] G. Tenti, C. D. Boley, and R. C. Desai, On the kinetic model description of Rayleigh–Brillouin scattering from molecular gases, Can. J. Phys. **52**, 285 (1974).

[20] A. S. Fernandes and W. Marques, Kinetic model analysis of time-dependent problems in polyatomic gases, Phys. A (Amsterdam, Neth.) **373**, 97 (2007).

[21] L. Wu, C. White, T. J. Scanlon, J. M. Reese, and Y. Zhang, A kinetic model of the Boltzmann equation for non-vibrating polyatomic gases, J. Fluid Mech. **763**, 24 (2015).

[22] Z. Gu and W. Ubachs, A systematic study of Rayleigh-Brillouin scattering in air, N_2, and O_2 gases, J. Chem. Phys. **141**, 104320 (2014).

[23] Y. Wang, Y. Yu, K. Liang, W. Marques, W. van de Water, and W. Ubachs, Rayleigh-Brillouin scattering in SF6 in the kinetic regime, Chem. Phys. Lett. **669**, 137 (2017).

[24] S. Chapman and T. G. Cowling, *The Mathematical Theory of Non-uniform Gases* (Cambridge University Press, Cambridge, 1970).

[25] B. Sharma and R. Kumar, Estimation of bulk viscosity of dilute gases using a nonequilibrium molecular dynamics approach, Phys. Rev. E **100**, 013309 (2019).

[26] C. D. Boley and S. Yip, Kinetic theory of time-dependent correlation functions in a binary gas mixture, Phys. Fluids **15**, 1433 (1972).

[27] J. R. Bonatto and W. Marques, Jr., Kinetic model analysis of light scattering in binary mixtures of monatomic ideal gases, J. Stat. Mech. Theory Exp. (2005) P09014.

[28] Z. Gu, W. Ubachs, W. Marques, and W. van de Water, Rayleigh-Brillouin Scattering in Binary-Gas Mixtures, Phys. Rev. Lett. **114**, 243902 (2015).

[29] Y. Wang, W. Ubachs, C. A. M. de Moraes, and W. Marques, Rayleigh-Brillouin scattering in binary mixtures of disparate-mass constituents: SF_6-He, SF_6-D_2, and SF_6-H_2, Phys. Rev. E **103**, 013102 (2021).

[30] B. L. Haas, D. B. Hash, G. A. Bird, F. E. Lumpkin, and H. A. Hassan, Rates of thermal relaxation in direct simulation Monte Carlo methods, Phys. Fluids **6**, 2191 (1994).

[31] I. D. Boyd and T. E. Schwartzentruber, *Nonequilibrium Gas Dynamics and Molecular Simulation* (Cambridge University Press, Cambridge, 2017).

[32] G. A. Bird, *Molecular Gas Dynamics and the Direct Simulation of Gas Flows* (Clarendon, Oxford, 1994).

[33] D. C. Rapaport, *The Art of Molecular Dynamics Simulation*, 2nd ed. (Cambridge University Press, Cambridge, 2004).

[34] W. Wagner, A convergence proof for Bird's direct simulation Monte Carlo method for the Boltzmann equation, J. Stat. Phys. **66**, 1011 (1992).

[35] I. D. Boyd, Computation of hypersonic flows using the direct simulation Monte Carlo method, J. Spacecr. Rockets **52**, 38 (2015).

[36] P. Valentini, P. A. Tump, C. Zhang, and T. E. Schwartzentruber, Molecular dynamics simulations of shock waves in mixtures of noble gases, J. Thermophys. Heat Transfer **27**, 226 (2013).

[37] S. J. Plimpton, S. G. Moore, A. Borner, A. K. Stagg, T. P. Koehler, J. R. Torczynski, and M. A. Gallis, Direct simulation Monte Carlo on petaflop supercomputers and beyond, Phys. Fluids **31**, 086101 (2019).

[38] D. Bruno, M. Capitelli, S. Longo, and P. Minelli, Monte Carlo simulation of light scattering spectra in atomic gases, Chem. Phys. Lett. **422**, 571 (2006).

[39] D. Bruno, A. Frezzotti, and G. P. Ghiroldi, Rayleigh–Brillouin scattering in molecular oxygen by CT-DSMC simulations, Eur. J. Mech. B/Fluids **64**, 8 (2017).

[40] D. Bruno, A. Frezzotti, and G. P. Ghiroldi, DSMC simulation of Rayleigh-Brillouin scattering in binary mixtures, in *30th International Symposium on Rarefied Gas Dynamics: RGD 30*, AIP Conf. Proc. No. 1786 (AIP, Melville, NY, 2016), p. 050011.

[41] C. Borgnakke and P. S. Larsen, Statistical collision model for Monte Carlo simulation of polyatomic gas mixture, J. Comput. Phys. **18**, 405 (1975).

[42] P. Valentini, C. Zhang, and T. E. Schwartzentruber, Molecular dynamics simulation of rotational relaxation in nitrogen: Implications for rotational collision number models, Phys. Fluids **24**, 106101 (2012).

[43] Z. Li, N. Parsons, and D. A. Levin, A study of internal energy relaxation in shocks using molecular dynamics based models, J. Chem. Phys. **143**, 144501 (2015).

[44] S. H. Jamali, M. de Groen, O. A. Moultos, R. Hartkamp, T. J. H. Vlugt, W. Ubachs, and W. van de Water, Rayleigh-Brillouin light scattering spectra of CO_2 from molecular dynamics, J. Chem. Phys. **151**, 064201 (2019).

[45] R. W. Boyd, *Nonlinear Optics*, 3rd ed. (Academic Press, New York, 2008).

[46] P. Atkins and J. de Paula, *Physical Chemistry: Thermodynamics, Structure, and Change*, 10th ed. (W. H. Freeman, New York, 2014).

[47] Y. Wang, Z. Gu, K. Liang, and W. Ubachs, Rayleigh-Brillouin light scattering spectroscopy of air; experiment, predictive model and dimensionless scaling, Mol. Phys. **119**, e1804635 (2021).

[48] W. M. Haynes, *Handbook of Chemistry and Physics*, 95th ed. (CRC Press, Boca Raton, FL, 2014).

[49] K. Koura and H. Matsumoto, Variable soft sphere molecular model for inverse-power-law or Lennard-Jones potential, Phys. Fluids A **3**, 2459 (1991).

[50] R. D. Trengove and P. J. Dunlop, Diffusion coefficients and thermal diffusion factors for five binary systems of nitrogen and a noble gas, Phys. A (Amsterdam, Neth.) **115**, 339 (1982).

[51] J. D. Anderson, *Hypersonic and High-Temperature Gas Dynamics*, 2nd ed. (American Institute of Aeronautics and Astronautics, Reston, VA, 2006).

[52] J. O. Hirschfelder, C. F. Curtiss, and R. B. Bird, *Molecular Theory of Gases and Liquids* (Wiley, New York, 1954).

[53] B.-C. Perng, S. Sasaki, B. M. Ladanyi, K. F. Everitt, and J. L. Skinner, A new intermolecular potential for liquid oxygen, Chem. Phys. Lett. **348**, 491 (2001).

[54] S. Plimpton, Fast parallel algorithms for short-range molecular dynamics, J. Comput. Phys. **117**, 1 (1995).

[55] J. G. Parker, Rotational and vibrational relaxation in diatomic gases, Phys. Fluids **2**, 449 (1959).

[56] J. A. Lordi and R. E. Mates, Rotational relaxation in nonpolar diatomic gases, Phys. Fluids **13**, 291 (1970).

[57] L. Monchick, K. S. Yun, and E. A. Mason, Formal kinetic theory of transport phenomena in polyatomic gas mixtures, J. Chem. Phys. **39**, 654 (1963).

[58] X.-D. Li, Z.-M. Hu, and Z.-L. Jiang, Continuum perspective of bulk viscosity in compressible fluids, J. Fluid Mech. **812**, 966 (2017).

[59] A. Gelb and R. Kapral, Rotational relaxation in the $Ar - N_2$ system, Chem. Phys. Lett. **17**, 397 (1972).

[60] P. G. Kistemaker and A. E. de Vries, Rotational relaxation times in nitrogen-noble-gas mixtures, Chem. Phys. **7**, 371 (1975).

[61] R. Holmes, G. R. Jones, N. Pusat, and W. Tempest, Rotational relaxation in helium + oxygen and helium + nitrogen mixtures, Trans. Faraday Soc. **58**, 2342 (1962).